THE BACKWATER EFFECT AS A TOOL TO ASSESS FORMATIVE LONG-TERM FLOOD REGIMES

F. X. Castelltort [1], E. Bladé [2], J.C. Balasch [1], M. Ribé [2]
[1]Department of Environment and Soil Sciences, Universitat de Lleida, Catalonia, Spain
[2]Flumen Research Group, Dept. of Hydraulic, Maritime and Environmental Eng., Universitat Politècnica de Catalunya, UPC, Barcelona, Catalonia, Spain
***Corresponding author*: F. X. Castelltort (xavier.castelltort@gmail.com)**

Abstract

The Ter River drains the south-eastern Pyrenees and flows into the Mediterranean Sea. A lithological constriction affects the normal water flow in the La Plana de Vic area. As a consequence of this disturbance in the flow, the shrinkage in the bedrock activates a backwater effect. Systematic water retention during extreme events has formative consequences. The process involves the creation of a helical flow for the structural misalignment of the channel at the point of narrowness. The backwater effect transmits the secondary currents backwards, resulting in the creation of a sinuous pattern upstream from the shrinkage. A tributary, the Gurri River, flows into the main river just before the constriction, and this too has been affected by the process of water storage and channel pattern change.

A two-dimensional numerical flow model (Iber) has modelled several hypothetical cases of flooding. This modelling aims to test the reach of the hydraulic influence upstream from the constriction, both in the main river and its tributary, due to the backwater effect. Moreover, it sought to find the best balance of discharge between the two streams. The upstream reach of the backwater effect was considered as its endpoint. During the flooding, the system reached hydraulic equilibrium between the constriction and the two endpoints when both were at the same water level, and the flow regime was subcritical everywhere. The hydraulic conditions that drove the water flow to the equilibrium are thought to be the ones that promoted formative processes in a sinuous pattern on a long-term basis.

The water discharge values obtained from this procedure are, in general terms, 50% above those considered to be a peak flood with a recurrence time of 500 years (Q_{500}), and they accomplish the conditions of extreme events. Thus classified, the calculated discharges can be helpful for comparison with those measured in historical and systematic records, because a water discharge like the one calculated has never been measured at the Ter River.

Key words: Ter River; lithological constriction; 2-dimensional numerical model; helical flow; Catalonia; Mediterranean river.

1. Introduction

One of the most frequently cited papers on meanders (Seminara, 2006) encourages the scientific cooperation of geomorphologists and fluid dynamists to solve a real challenge for future research: understanding the mechanics of meander formation in purely cohesive environments driven by the three-dimensional structure of the flow field. The author recognises the capacity of geomorphologists in extracting the general behaviours of

nature from field observations as well as the ability of fluid dynamists to quantify them and develop theoretical analyses.

The aim of this paper is based on the collaboration between the two scientific branches. Geomorphologists have identified a field example of the backwater effect caused by lithological constrictions. The geomorphological setting demonstrates a point where meander initiation could be quantified, while fluid dynamists corroborate the hypothesis. The second step – the core of the paper – would be to profit from the circumstance and develop a hydraulic strategy to assess average discharge during flood events in the past.

One of the factors that modifies the flood hydrograph shape is the backwater effect created by introducing water storage upstream from a flow disturbance. The backwater effect, due to artificial interventions in rivers such as bridges or spurs, has been studied extensively (for instance, Naudascher and Medlarz, 1983; Azinfar and Kells, 2011; Hidayat et al., 2011; Saif and Hosoda, 2012; Brandimarte and Woldeyes, 2013; Luo et al., 2018). However, limited number of studies investigated the backwater effect caused by geomorphological constrictions and its consequences on river morphology. Water storage attenuates the peak of the flood wave. From this point of view, the backwater effect and water storage are involved in flood routing and travelling flood wave propagation. The backwater effect impacts flood routing in a significant way, leading to a loss of water energy due to a flow blockage and the backing up of the water behind a constriction (Chow, 1959). There are a significant number of previous scholars that analyse the backwater effect for different situations, however, in most cases, they focus on one-dimensional problems and utilise the energy equation for its mathematic description. Despite this, it has been long known that the backwater effect, especially for non-stationary flows, can be explained using the theory of Characteristics for the hyperbolic systems of equations (Stoker, 1957; Toro, 2001), as did De Vriend (1987) to study morphological evolutions in shallow waters. It is worth noting that the Characteristics theory, or Bicharacteristics in two dimensions, is the base for several modern numerical schemes that are used to solve shallow water equations by means of the finite volume method (Vázquez-Cendón, 1999).

The backwater effect completely changes the flow regime not only downstream from the constriction but, more significantly, upstream from it. The volume of the stored water flowing through the basin outlet, influenced by the angle between the channel reach before and after the constriction, creates a new three-dimensional helical flow structure that can be transmitted upwards, owing to the low flow regime established by the backwater effect, and that is partly responsible for the sinuous planform of the channel.

The case of a backwater effect due to lithologic constrictions into the channel maintains the same result over the flow. The results of the iterative water storage are formative, and the magnitude of the river pattern change in the affected area correlates with the average flood wave arriving towards it. The strategy involves modelling and evaluating the reach of the backwater effect upstream from the constriction and then converting it into an average flood peak.

The awareness of the upstream reaching of the endpoint of the backwater effect would be significant. In this regard, a sensitivity analysis at the channel constriction, obtained by

applying different water stages as internal conditions in a numerical flow model, would allow to find out the upstream influence of lithological constrictions. The upstream point, where all water levels converge, is considered as the endpoint. This point, concerned with the process of backing up the water to be formative, must coincide with a relevant geomorphic point, linking hydraulics with geomorphology. The conceptual model proposed is based on the repetition of the backwater effect in a river reach upstream from a channel narrowness. Successive and discontinuous floods arriving at this point generate helical flow structures that create a pattern of channel sinuosity according to the average flood peak arriving at the constriction as well as the volume of the water backed up.

The result of the backwater effect upstream from a constriction is a new sinuous channel pattern. Several research studies have been conducted on meandering, most of which deal with the temporal and spatial evolution of meanders on non-cohesive banks (for instance, Ikeda et al., 1981; Parker et al., 1982; Johannesson and Parker, 1989; Stolum, 1996; Seminara et al., 2001; Zolezzi and Seminara, 2001; Edwards and Smith, 2002; Hooke, 2003, 2007; Camporeale et al., 2005; Lanzoni and Seminara, 2006; Seminara, 2006; Camporeale et al., 2007; Braudrick et al., 2009; Crosato, 2009; Frascati and Lanzoni, 2009, 2010; Güneralp and Rhoads, 2009; Howard, 2009; Pittaluga et al., 2009; Blankaert and Vriend, 2010; Hooke et al., 2011; Pittaluga and Seminara, 2011; Seminara and Pittaluga, 2012; Ottevanger et al., 2013; Vermeulen et al., 2016). The common feature in all these works is the presence of helical flows, or, in other words, the extensive development of secondary flows.

There has been comparatively less investigation on meander initiation or formation. Leopold and Wolman (1960, and references therein) stated that the impact of helical flow led by flow instabilities is the dominant factor of meander initiation. Parker (1976) proposed a third effect in addition to the potential (inertial and gravitational) and the friction factors: the sediment transport for alluvial streams, the Coriolis acceleration for oceanic currents, and the heat differences for glacial meltwater streams. Howard and Knutson (1984) suggested that a meandering pattern is produced starting from an initially straight channel with small random perturbations. Blondeaux and Seminara (1985) suggest a phenomenon of resonance, connected with bar instability in some sense and associated with meander formation. Schumm et al. (2000) confirmed a different development of the meanders at both sides of the contact of variable resistance materials. Lazarus and Constantine (2013) suggested the concept of flow resistance (R), represented by the landscape roughness attributable to topography or vegetation density and relative to the surface slope (S), proposing a ratio R/S, which would exert a primary landscape control on path sinuosity. This concept would be independent by the internal flow dynamics. Resistance-dominated surfaces would produce channels with higher sinuosity as compared to those of slope-dominated surfaces, because increased resistance impedes downslope flow. This author admits that R/S derives from the Froude number, which can also be expressed through slope and resistance. In this respect, the backwater effect can be understood as a kind of flow resistance that modifies the flow regime reducing the Froude number to a significant degree.

The subject of this research is to find the equilibrium between hydrodynamics and geomorphology upstream from a lithological constriction. This equilibrium depends on

the backwater effect produced by the water discharge of the two rivers joined upstream from the constriction. Both the hydraulic endpoints at the equilibrium coincide with a relevant geomorphic feature, which is the ending (or the beginning) point of a meander. During the process of flooding, at the equilibrium**,** the two points must be at the same water level. Moreover, there cannot be any change in the flow condition between the constriction and the endpoints, which implies that there can only be two control sections, one at the endpoint and the other at the constriction. At this time, modelling permits to know the water discharge peak from both rivers as well as the water storage.

2. Regional setting

The process of the formation of a sinuous channel pattern upstream from a lithological constriction has been identified in a Mediterranean river, the Ter River and its tributary, the Gurri River. The Ter River flows from its headwaters in south-eastern Pyrenees into the Mediterranean Sea. It is the primary river of the Internal Catalan Basins, which is 208 km long and has a catchment of 2960 km^2. Regarding the course of the river and basin hydrology, three parts integrate its drainage basin: the Upper Ter (length: 50 km; basin surface: 691 km^2; mean gradient of 3%), the Middle Ter (length: 90 km; basin surface: 1057 km^2; mean gradient of 5.4‰), and the Lower Ter (length: 68 km; basin surface: 1212 km^2; mean gradient of 2.3‰). The area of study is situated in the Middle Ter, where the river length is 91 km, the basin surface is 1529 km^2 (250 km^2 from the Gurri river basin) and the mean gradient is 1.8‰. The Ter River headwaters form the boundary between the French and the Catalan Pyrenees, with highs near 3000 m asl. The Upper and Middle Ter are two of the rainiest areas in Catalonia: the mean annual precipitations range between 900 and 1200 mm. The mean annual water discharge of the river at Roda de Ter gauge station was found to be 17 m^3/s. There are no significant reservoirs upstream from the constriction, but the Ter River is one of the most micro-regulated rivers by weirs in the Iberian Peninsula that have supplied water to riverside industries since the mid of 19^{th} century. The central city of the Upper Ter is Ripoll, situated 700 m asl, and the main city of the Middle Ter is Vic, located at 500 m asl (Fig. 1).

One of the most extreme floods in the NE of the Iberian Peninsula in the last century occurred in October 1940 and affected the Upper Ter (Becat and Soutadé, 1990). The French watershed registered over 1000 mm of rain in a day and 800 mm in the Catalan Pyrenees. The peak discharge of this event in the study area was 2350 m^3/s just after the confluence.

The primary hydrological parameters of the Ter River and its tributary, the Gurri River, are depicted in Table 1 (Catalan Water Authority, 2017), resulting from a statistical analysis of daily water discharges at the gauging station of Roda de Ter (Fig. 1) using the statistical extreme values distribution SQRT-ET-max (Etoh et al., 1986) – the one adopted by the Catalan Water Authority.

	Ter River before the confluence	Gurri River	Ter River after the confluence
Q_{500}	3440 m^3/s	1264 m^3/s	4610 m^3/s
Q_{100}	1962 m^3/s	652 m^3/s	2605 m^3/s
Q_{50}	1454 m^3/s	510 m^3/s	1904 m^3/s
Q_{10}	562 m^3/s	158 m^3/s	714 m^3/s
Mean annual water discharge (1927–1990)			17.16 m^3/s

Table 1. Principal hydrological parameters of the Ter river before and after the confluence with the tributary, the Gurri River (Catalan Water Authority, 2017). Values of Q_{10}, Q_{50}, Q_{100}, and Q_{500} are water discharges, with return periods of 10, 50, 100 and 500 years respectively.

Montalbán et al. (1994) published water discharges of this particular station. This publication includes a compilation of 55 years of maximum annual water discharge. The average value is 531 m^3/s, with a standard deviation of 492 m^3/s. Using these data and the Gumbel distribution, it can be inferred that Q_{500} is 2914 m^3/s. In this research we used a higher value of 3440 m^3/s for two reasons: 1) the values obtained with SQRT-ET-max distribution are slightly larger than those with Gumbel for low frequencies; 2) 1994 data series have extended for over 20 years. Nevertheless, based on the public data available in Montalbán et al. (1994), it can be deduced that the value of Q_{500} in the article is realistic. Moreover, the Ter River basin is situated on the Mediterranean coast, where hydrologic regimes are highly irregular and torrential, and such high values of specific water discharges are not unusual (Pino et al., 2016).

In the La Plana de Vic area, the Ter river's course has a north-south direction through a strike valley, developing a sinuous pattern (Fig. 1). In this area, the river bends to the east until it flows into the sea. After this bend, a tributary, the Gurri River, flows through the strike valley from south to north into a predominantly straight channel pattern until near the confluence point, where it becomes sinuous. The meanders of the Ter and Gurri rivers are incised into a cohesive bedrock, that is formed by the Eocene grey marine marlstones and is underlain by a harder unit of sandstone that shapes the constriction and makes the dip slope of the strike valley. The Ter River incises into this more resistant unit thereby forming the gorge. It leaves the strike valley as it incises into a homoclinal Paleogene sedimentary succession, tilted towards the west. The entrance to the canyon becomes a significant channel constriction due to this lithological change. Two different incised channel patterns can be identified in the Ter River before and after the constriction. An incised meandering style over the less resistant material and an incised sinuous pattern over the more resistant material can be observed. The straight stream segments incised into the resistant rock layer are related to a fault lineation. Before the constriction also the tributary flow along a meander that has a shape comparable to the meander existing along the Ter River.

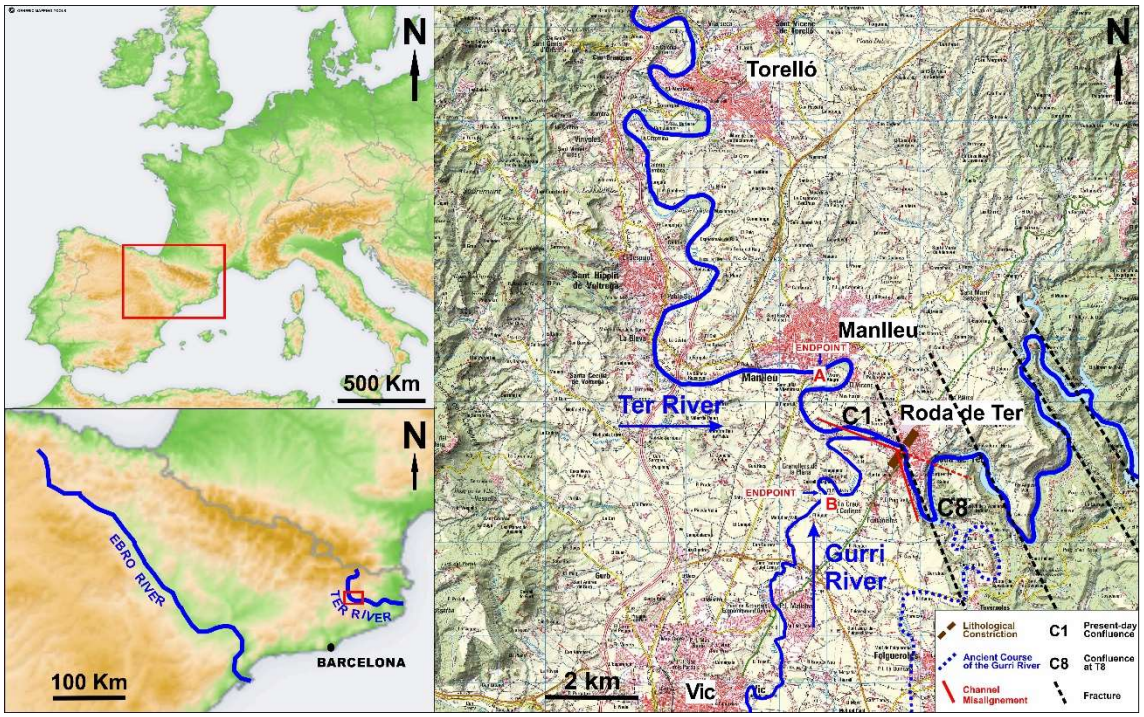

Fig. 1. Map of the location of the Ter River in the Iberian Peninsula and the layout of the river with its tributary, the Gurri River, in La Plana de Vic area. Both rivers flow along a strike valley in opposite senses, and after the confluence, the Ter River leaves the valley through a gorge initiated by a lithological constriction. Original map from the Spanish Geographic Authority (IGN).

The difference in shape and sinuosity between the river bends before and after the constriction is noticeable (Fig. 1). Before the constriction, the river flows for a distance in a meandering pattern with a sinuosity of 1.75, but it reaches a high degree of sinuosity (3.1) after the constriction, even though the channel planform does not follow the classical meandering pattern. This style implies a certain degree of lateral channel migration even in incised channel scenarios, which is not the case here. After the constriction, a family of basement faults of NW-SE direction that continued in the cover distributes over the resistant unit. The Ter River adjusted its course to this fracture lineation, demonstrating an incised sinuous channel unaffected by any lateral migration. The river flows through the sinuous gorge for a distance of 17,300 m. This long route, with its narrowness and great sinuosity, reinforces the impact of the constriction on the flow routing of the river's floods.

A detailed mapping of the study area (Castelltort, 2017a) represents the Quaternary succession of the Ter river's terraces in the La Plana de Vic area (Fig. 2). The author has surveyed up to ten strath terrace levels. Terrace surfaces are identified alphanumerically, with the lower number (T1) referring to the Holocene deposits, up to 5 m thick, over the channel floor. Pleistocene terraces depict in the map a meandering pattern. The Holocene terrace meanders through the present-day floodplain incised into the strike valley. The Holocene terrace and a narrow lateral remnant fringe of T2 (15 m above the channel floor) are the only two terraces into the incised meandering floodplain. T3 (30 m above the channel floor) is always out of the incised floodplain. This fact supports the notion that the current meandering floodplain is related to Holocene or T2. Older terraces, from T3 to T10 (140 m above the channel floor) are not related to the current channel course.

The last reach of the river before the constriction, that flows on the less resistant unit, diverts 50º towards the south after the constriction (Fig. 1, line in red), because when entering the gorge, it flows over a fracture that constrains its route. At the end of this reach an ancient confluence of the main river and its tributary is present (C8 in Fig. 1). The presence of a set of abandoned incised meanders within the more resistant unit allows the main course to follow the old course of the tributary. The age of this paleo-confluence is related to the terrace T8 (76 m above the channel floor). The confluence migrated from point C8 to C1 due to the homoclinal shift of the strike valley, which implied a distance of 2500 m to the north-west and an incision of 76 m (Castelltort et al., 2017b).

The first meander of the main river, upstream from the constriction, has a wavelength of 1600 m and sinuosity of 2.35. The first half-meander has a radius of curvature of 600 m bending in a clockwise direction, while the second half-meander has a radius of curvature of 350 m.

The tributary develops a meander upstream from the confluence with a wavelength of 1000 m and sinuosity value of 2.2. The first half-meander has a radius of curvature of 350 m bending in a clockwise direction, while the second half-meander has a radius of curvature of 150 m. The endpoints of the two meanders upstream the constriction have the same altitude: 441 m asl (points A and B in Fig. 1).

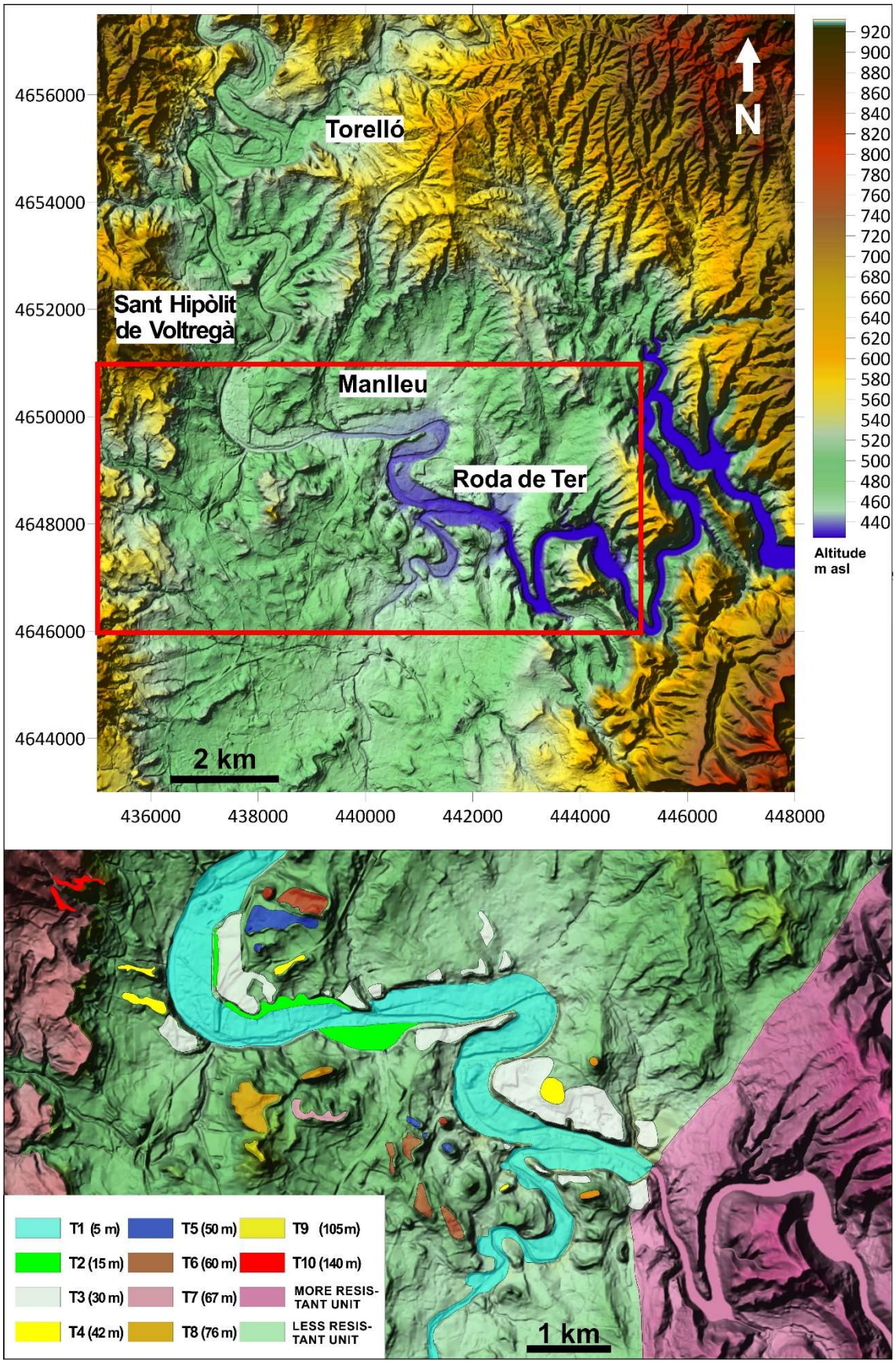

Fig. 2. Terrace remnants of the Ter River in La Plana de Vic area. Terrace surfaces are identified alphanumerically, with the lower number (T1) used to represent the Holocene surface. Numbers indicate terrace altitude above the channel floor. Adapted from the Catalan Geographic Authority (ICGC).

3. Materials and methods

3.1 Modelling

The freeware package Iber (www.iberaula.com; Bladé et al., 2014a) was used in this research for numerical flow modelling. It is based on the solution of the two-dimensional shallow water equations using the finite volume method (Vázquez-Cendón, 1999) and the numerical scheme of Roe (1986). The reader is referred to Bladé et al. (2014a) and the references therein for a detailed description and experimental validation of the numerical schemes used to solve the shallow water equations, which have been excluded here for the sake of conciseness. This hydraulic modelling tool has been applied in several studies in the past, including river inundation modelling (Bladé et al., 2014b), overland flow (Cea and Bladé, 2015), evaluation of gully restoration measures (Castillo et al., 2014), wood transport in rivers (Ruiz-Villanueva et al., 2014), and water quality (Cea et al., 2016). In the context of the present work, the Iber software has been used to demonstrate the early formation of meanders upstream from a constriction to some extent.

Mesh preparation is one of the most important tasks that must be carried out to achieve reliable results. A 15x15 m DEM, with a vertical accuracy of 0.9 m, from the Catalan Geographical Authority (2017) was used in this study. A recent photogrammetric terrain survey from an aircraft was the source of the digital model, hence, it contains several anthropic structures that would distort the results. Anyhow, as the research aims to conduct numerical modelling through the most unaltered environment, thus, anthropic structures such as canals, bridges, dams, weirs, and the static pool level of the tail-end of a reservoir were deleted. The software Surfer 14 (Golden Software, 2017) fulfilled this purpose.

With the occurrence of extreme floods, the overland flow completely inundates floodplains. Riparian forests have historically covered these areas and are a significant factor in flow retarding. A Manning's roughness coefficient of 0.070 – a weighted average value between that of a channel zone (0.040) and a floodplain bush area (0.080) – was primarily used. These values have been calibrated with data from a historical flood in the meandering reach of the Ebro River (Ruiz-Bellet et al., 2017). However, other scenarios of global roughness were considered, from an area bare of vegetation to an afforested floodplain. Therefore, the modelling was run applying a range of Manning's coefficients (0.04, 0.06, 0.07, 0.08) and, on one occasion, a multiarea coefficient of roughness (0.04, 0.08).

With the aim of avoiding boundary effects in the modelling, the study area included several kilometres upstream and downstream from the involved constriction. The long route of the flow through the gorge was entirely included in the modelling, as it contributes to the flow retardation in the constriction. Water discharges, inflowed in the model to analyse the maxima, were continuous, reported in Table 2, as they were considered as scenarios of extreme events with low probability of occurrence.

3.2 Performed hydraulic tests

3.2.1 Meander formation upstream from the constriction

A numerical model of a simplified geometry was built based on this case. The geometry consists of the flow constriction at the exit of a broader straight channel pattern. The channel reach downstream from the constriction does not align with the previous, and the deviation angle is 50° (Figs. 1 and 3A). The constriction can exert a double influence, generating secondary flows by the lack of alignment between the channel reaches before and after it, and changing the flow regime upstream from it due to the backwater effect. This test aims to verify if secondary flows are generated through the change in downstream channel orientation due to bend instability, as stated by other authors (Ikeda et al., 1981).

It is a known fact that secondary currents, or helical fluxes, triggered by bed resistance or river curves are responsible for meander formation (Leopold and Wolman, 1960; Ikeda et al., 1981). The impact of these currents is that flow velocity has a component towards the outer bank at the water surface, while there is a deflection from the main channel axis direction towards the inner bank at the bottom. This process explains meander migration, erosion of the outer bank, and deposition at the inner bank. Two-dimensional numerical models cannot describe the precise patterns of 3-dimensional helical fluxes, but the effect of these secondary currents, which depends on the radius of curvature of the flow streamlines, can be added to the shallow water equations. This is commonly done through additional shear stress terms, that depend on the radius of curvature (Baghlani, 2012; Rinaldi et al., 2008). Moreover, it is possible to estimate the deviation angle of the near-bed flow concerning the mean flow (Deltares, 2014; Vasquez et al., 2005). The formulation of these four references was added to the source code of Iber, and together with its sediment transport module, the case allows the analysis of the morphological evolution of the simplified geometry presented in Fig. 3A. Moreover, another numerical model of a simplified geometry was built with a narrow channel reach after the constriction, completely aligned with the previous one, to verify if Coriolis' force was able to produce helical flow and initiate meander formation on its own. Iber integrates a module of Coriolis' force in its code.

3.2.2 Convergence analysis

The next test applied to the channel constriction was a convergence analysis. It involves imposing varying water depths as internal conditions at the constriction in the flow model. Water depth profiles resulting from every modelling were plotted on a graph. The point, upstream from the constriction, where the profiles converge, marks the extent of the zone hydraulically influenced by the constriction. If there was no upstream hydraulic influence, profiles convergence would not occur: the test is based on the control section concept (Chaudhry, 2008) and the Characteristics theory (Stoker, 1957; Toro, 2001). The constriction controls the flow condition, maintaining a subcritical flow upstream from it, and an upstream channel section controls the flow condition at the convergence point (the endpoint) if the arriving flow is supercritical. Any perturbance in the flow can be transmitted upstream due to its subcritical regime.

The test aims to find out the hydraulic influence of the constriction and to assess the upstream reach of this influence, which would be the endpoint of the backwater effect. The location and water level of this point can be used in a flood routing model to obtain

the water storage volume. In practice, the fluctuations in water depth profiles can appear in the results of the test solely due to the location of the profile trail created in the channel reach to conduct the hydraulic analysis. Besides this, the relevant result is the point where all water depth profiles converge.

3.2.2.1 Convergence analysis in the Ter River

The convergence test was applied to the constriction in the Ter River, with a Q_{500} water discharge (3440 m^3/s) in the flow model. Three water elevations were used as internal conditions in the constriction: 436, 440, and 444 m asl. The results plotted the water depth profiles on a graph. All the profiles must converge upstream from the constriction at the endpoint due to the backwater effect. In a geomorphological context, this hydraulically calculated point should coincide with a significant point on the meander. This is the location where, upstream from the constriction, the first meander ends.

3.2.2.2 Convergence analysis in the Gurri River

A Q_{500} water discharge of 1250 m^3/s was inflowed in the flow model only into the Gurri River, since the channel constriction influence can arrive in the tributary as well. As an internal condition, the water elevations applied to the constriction were the same as in the case of the main river: 436, 440, and 444 m asl. As stated before, the convergence point should coincide with a significant point in the tributary's meander, upstream from the constriction.

3.3 Flood modelling in the two rivers

First, two Q_{500} discharges were inflowed separately into the main river as well as the tributary, with the aim of evaluating the upstream reach of the backwater effect produced by them. As a result of the convergence analysis, it was thought that a particular water level, where changes in flow condition disappear, would be found by modelling different flood cases by trials and errors. At this water level, the lithological constriction should appear as a control section. The flow condition is controlled both at the constriction as well as at the upstream endpoint, and at this stage, the pool level of the virtual reservoir should be reached. Local phenomena (Chow, 1959), such as hydraulic jumps and drops, may appear in the flow model, because the water level is below the assumed virtual pool level. These appear in the inflexion point area between the first and the second half-meanders, because streamlines cross the areas of channel and floodplain under the critical depth.

3.4 Profile analysis

It is worth plotting the water elevation profiles to find out the water storage distribution in the virtual reservoirs that developed upstream from the constriction. Additionally, the analysis of the profiles would show the endpoint position. The backwater effect forms flat-water elevation profiles behind the lithological constriction. However, if the inflowed water discharge is under the value in which the constriction functions as a control section until the endpoint, the aforementioned local phenomena appear between the areas of water storage. This means that the changes in flow regime from subcritical to supercritical or

vice versa take place between these areas. This corresponds to unbalanced situations between the constriction and the endpoints as well as between the water level at both endpoints. Water profile analyses aim to find a state of equilibrium between the two endpoints and the constriction, because this circumstance is thought to be created on a long-term basis by the reiteration of floods arriving at the constriction.

4. Results and discussion

4.1 Meander formation upstream from the constriction

The main aim of this simulation was to analyse if the numerical model can help in understanding the formation of the present meandering pattern. The application of Coriolis' module in the numerical model with fully aligned channel reaches – before and after the constriction – did not yield any results regarding helical flows. Streamlines appear symmetrically at both sides of the channel axis. The Coriolis' force on its own seems to be irrelevant in meander initiation in this case study.

The results indicate that the skewness of the gorge downstream from the constriction triggers a helical flow. Figure 3 depicts the water surface streamlining at the constriction (Fig. 3B), compared with near-bed streamlines (Fig. 3C) and it documents that the deviation occurs due to secondary currents. Another effect of secondary currents is that bedload transport does not follow the mean flow direction and instead follows the near-bed velocity direction thereby increasing erosion at the outer part of the curve and favouring sedimentation at the inner part.

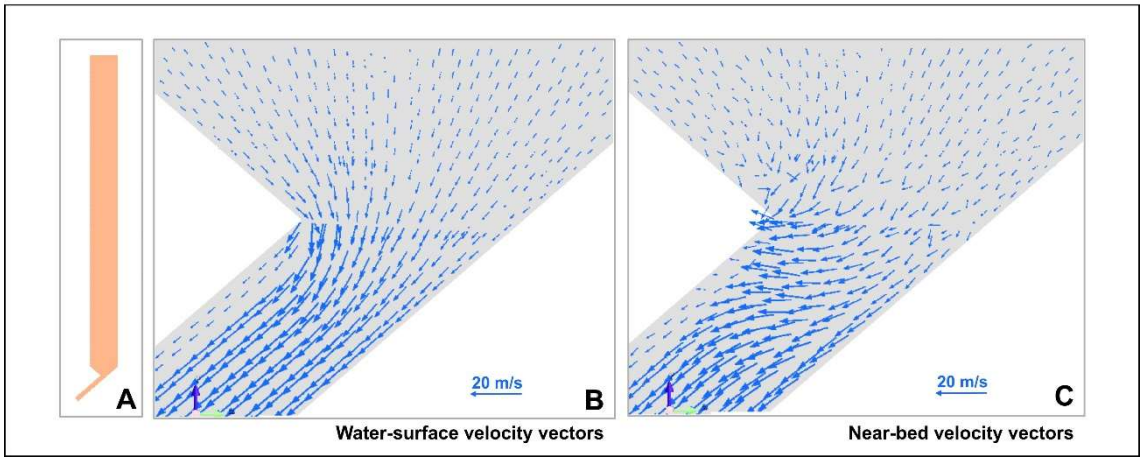

Fig. 3. A: Outline of the entire geometry of the simplified model. The channel is 4000 m long and 400 m wide. The lithological constriction is 100 m wide; B: Water surface velocity distribution at the constriction of the simplified numerical model; C: Near-bed velocity in the same area.

Additionally, since the flow is subcritical, the backwater effect at the constriction is affected by its secondary flow. The effect upstream from the constriction, even with an initial symmetrical channel bottom in the wide river reach, would not be symmetrical with respect to the river axis. Moreover, the asymmetry in hydrodynamics induces asymmetry of the bedload transport, impacting the evolution of the bed elevation (Fig. 4A and 4B).

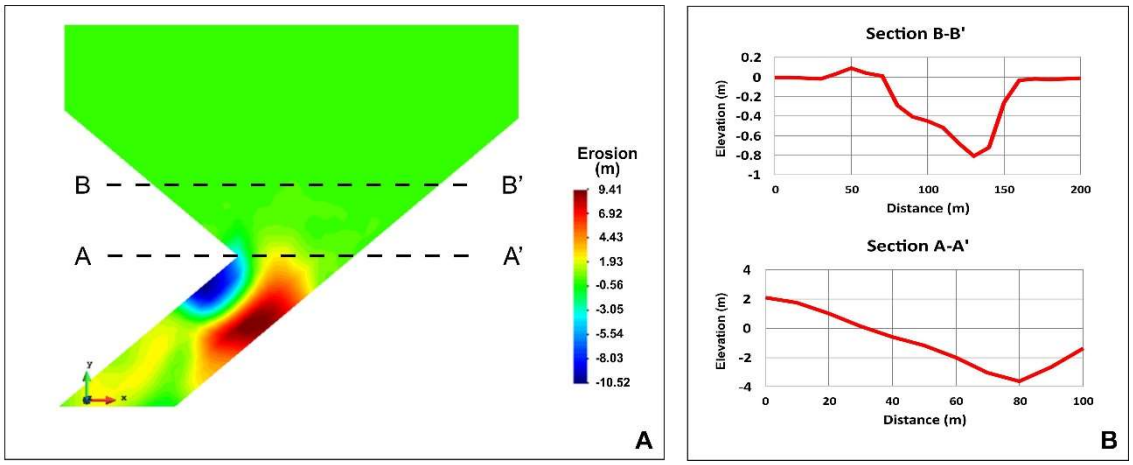

Fig. 4. A: Numerical results of erosion/deposition patterns at the constriction after a 10-day simulation; B: Bed elevation at cross section A–A' and B–B' after a 10-day simulation. The negative numbers indicate sedimentation.

The results of the meander formation modelling aligned with those obtained by other authors. Leopold and Wolman (1964) speculate how chance perturbations of the flow may persist and lead to the development of a sinuous pattern. This case answers the authors' question: flow perturbation persists because its origin is structural and the constriction is a structural landform, including a lithological contrast and a fracture lineation. Schumm et al. (2000) speculated about the occurrence of resistant materials in the channel, and they concluded that bedrock can confine the channel and, at the same time, retard meander shift and bank erosion. They predicted meander deformation or compression upstream from a bedrock of contrasting resistance. Blondeaux and Seminara (1985) supported the notion that resonance controls bend growth. In the present case, resonance phenomena are necessary for meander development, but they have to operate upstream, according to the action of the Characteristics theory, for which the backwater effect must create an ideal environment. The upstream migration of meanders was discussed by Seminara (2006) under super-resonant conditions by crossing a resonance barrier. These conditions are encountered in nature (Zolezzi and Seminara, 2001), and the present case can be considered as an example of this. The concept of flow resistance (R) proposed by Lazarus and Constantine (2013) could be applied to the meanders of La Plana de Vic area. The constriction and the change in the orientation of the river redirect a strike stream to an anti-dip stream, seeking the drainage basin outlet, and contribute to increasing the R. Nevertheless, the isolated meanders related to the constriction would require to be separated from those related to the bend that changes the flow direction of the river. The meander belt in the strike valley has a different origin.

4.2 The convergence analysis

A convergence analysis was carried out in the Ter river's course between the constriction, and upstream, in the locality of Manlleu (Fig. 1). A Q_{500} water discharge of 3500 m^3/s was inflowed to confirm the hydraulic influence of the lithological constriction at Roda de Ter (Fig. 1). This test was conducted to obtain evidence of the upstream reach of the backwater effect in the constriction and locate the endpoint of the effect. The reach of the hydraulic influence arrives 5300 m upstream, which is the hydraulic endpoint, as depicted in Figure 5. The geomorphic endpoint does not coincide with the hydraulic endpoint,

located 4525 m upstream from the constriction. At this site, the difference in depth between the three profiles is 0.88 m. However, the geomorphic endpoint was considered in the results for practical purposes.

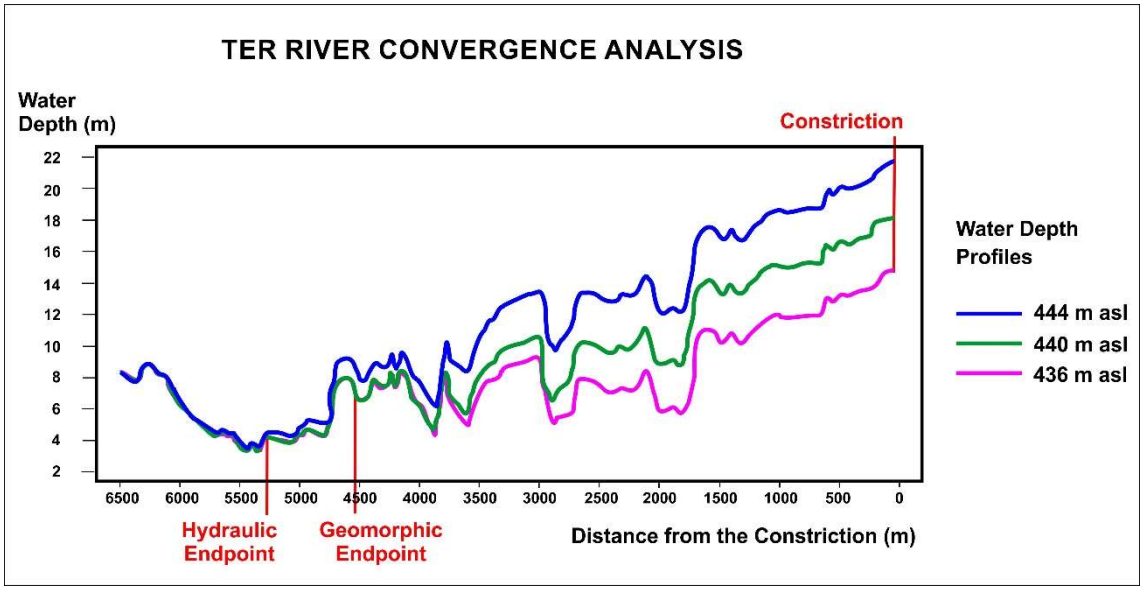

Fig. 5. Analysis of convergence performed in the Ter River from the lithological constriction to 6500 m upstream. Three water elevations were imposed in the constriction as internal conditions in the flow model to evaluate the upstream reach of the constriction influence in the Ter River's channel. The graph plots depth profiles of every modelling. The hydraulic endpoint of the backwater effect locates 5300 m upstream from the constriction. The geomorphic endpoint lays 4525 m upstream from there.

The same test has been applied to the Gurri River (Fig. 6). In this case, a near Q_{500} water discharge of 1250 m^3/s has been inflowed. The backwater effect initiated in the constriction by the tributary's flood should reach to the hydraulic endpoint of this river, which should coincide with its geomorphic endpoint, at the end of the meander. The modelling has collocated the hydraulic endpoint 750 m upstream from the geomorphic one. The hydraulic endpoint is located 4750 m upstream from the constriction. Nevertheless, the water level at the geomorphic endpoint only varies 0.02 m between the three tests. This is a minimum variation between the two locations and for practical purposes, it has been considered the end of the meander the location of the endpoint, which is 4000 m far from the constriction.

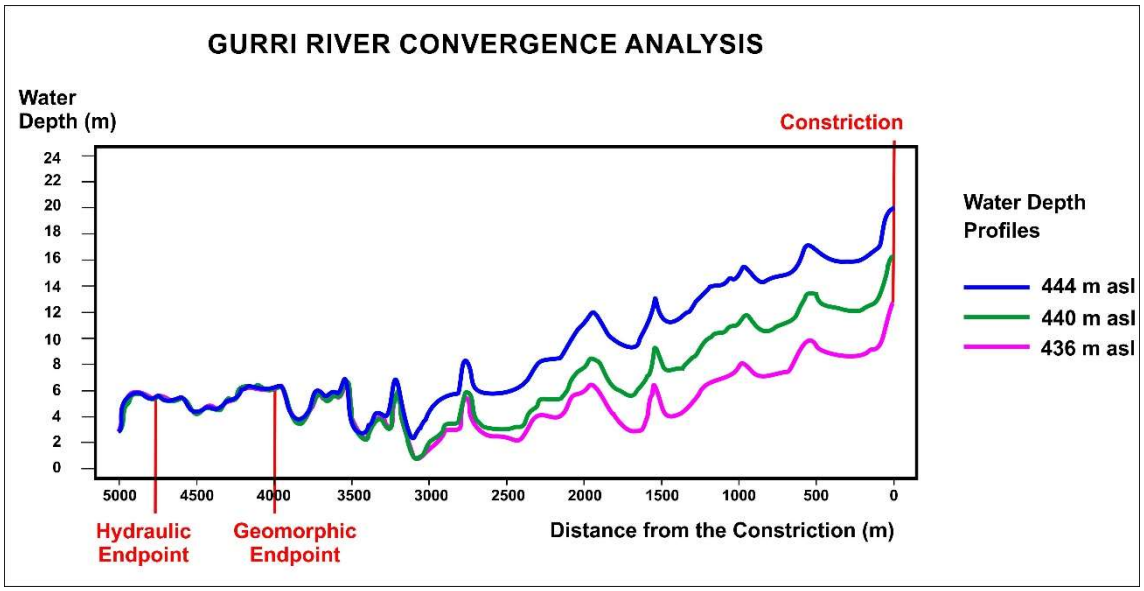

Fig. 6. Analysis of convergence performed in the Gurri River from the constriction to 5 km upstream. Three water elevations were imposed in the constriction as internal conditions in the flow model to evaluate the upstream reach of the constriction influence in Gurri river's channel. The endpoint of the backwater effect is located hydraulically 4750 m upstream from the junction.

4.3 Hydraulic dynamics of the two rivers

The Ter and Gurri rivers run parallel for about 950 m before the confluence. At a low stage, the tributary flows into the main river 560 m upstream from the constriction while, at a high stage, the confluence point is located at 1500 m (Fig. 1).

Four flow situations can occur at this river junction:

(1) Both rivers are at a low stage, and the confluence is located 560 m upstream from the constriction. In this situation, the two rivers flow parallelly for nearly 1000 m before the confluence. This condition does not generate significant consequences.

(2) The Ter River is at a low stage, and the Gurri River is at a high stage (Q_{500}; 1250 m^3/s). The tributary flows into the main river at a point between 427 and 441 m asl of elevation, depending on its stage of flooding. When a tributary's flood wave at a given discharge arrives at the constriction, the backwater effect will be dependent on the rating curve in the constriction, because the tributary's discharges would be lower than those of the main river. The effect on the backwater will remain minor. The most significant feature of this flow model is that the backwater effect produced by the tributary's flood flows upstream to the inflexion point in the main river's meander. Regarding the zone of Froude number near to 1 in the tributary's meander, local phenomena would be located at the inflexion point.

(3) The Ter River is at a high stage (Q_{500}; 3550 m^3/s), while the Gurri River is at a low stage. The backwater effect is initiated when the main river's flood wave arrives at the constriction and depends on its water discharge: the greater the water discharge, the more significant the impact of the backwater. Part of the backed-up water will flow upstream into the tributary's channel, depending on the amount of the main river's water discharge. Since the tributary is at a low stage, its water level depends on the main river's backwater

effect. Subsequently, the tributary's water level is dependent on the rating curve of the main river's flood at the constriction.

Local phenomena do not occur in the tributary, because it is at a low stage and flows in a subcritical state. These phenomena tend to develop at the inflexion point of the main river's meander and at its endpoint. At the inflexion point, flowlines cross the areas of floodplain where the water depth is lower than the channel depth. An increase in water depth implies a change in the channel section as well as the flow regime.

(4) Both the rivers are at a high stage. This situation is common when both rivers have a large flood peak. Although a peak flow of the main river arrives later to the confluence it imposes the water level in extreme events, affecting the regular inflow of the tributary. The constriction promotes the effect upstream from the main river, and its rising water level extends the consequence to the tributary's channel, depending on its water discharge (Fig. 7).

Various cases have been modelled (Table 2). The case of two Q_{500} (3550 m^3/s + 1250 m^3/s) from both rivers represents nearly the same value of recurrence in the constriction, which is a peak flow of 4800 m^3/s. The results are depicted in Figure 7, where the water level layer and the values of significant points are displayed on the right and the Froude number layer and its values on the left.

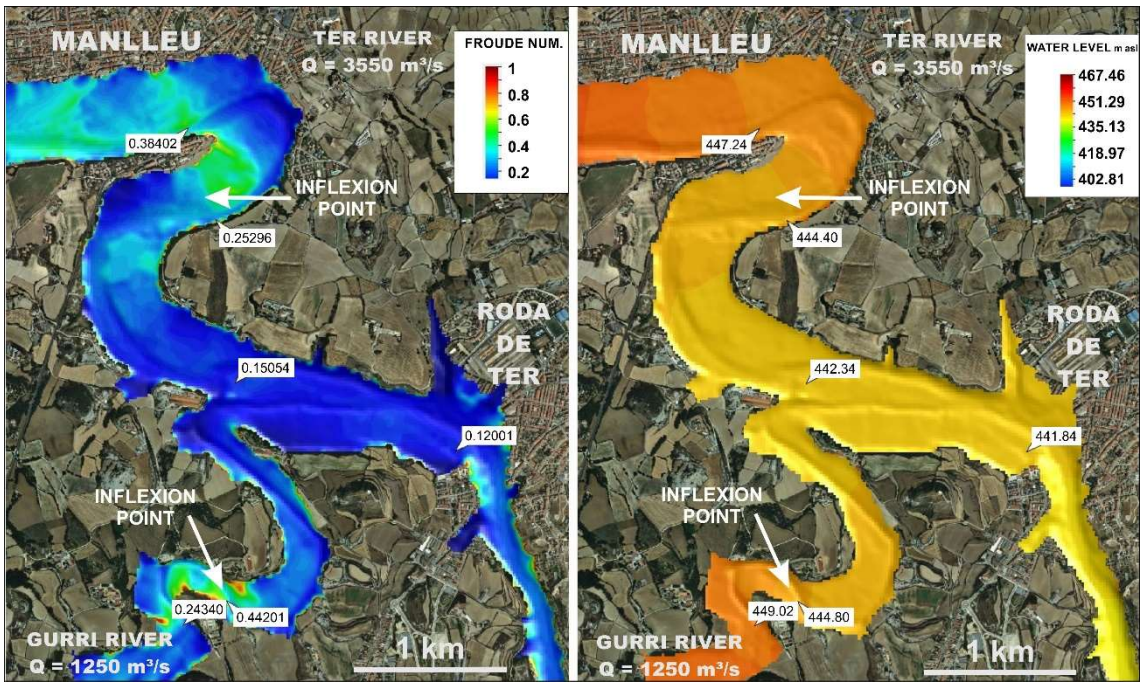

Fig. 7. The two rivers are at a high stage (Q_{500}). The discharges pattern appears to be at equilibrium, but water elevations in the areas of the endpoints are not balanced. Besides, local phenomena are clearly developed at the inflexion points.

An analysis of this situation exhibits different aspects: water level at the endpoint of the tributary channel is 2 m higher than it is at the endpoint of the main river channel. This demonstrates a certain disequilibrium between both discharge patterns in favour of the tributary. The reach of the backwater effect confirms the disequilibrium. The discharge

from the main river has to increase in order to establish hydraulic equilibrium between the discharges of the two rivers.

At the Q_{500} discharge pattern, the backwater effect only reaches the inflexion point of the two meanders (Fig. 8). At a high stage, flow condition varies in the limits of both half-meanders due to flowlines coming from a channel reach, cross the floodplain area at a lower water depth, and returning to the channel, which is at a higher water depth. Flow depth decreases over the floodplain areas, and local phenomena develop if this depth is lower than the critical depth. At this water discharge pattern, the two rivers flowing at Q_{500} and the planform and profile of both meanders are not in equilibrium.

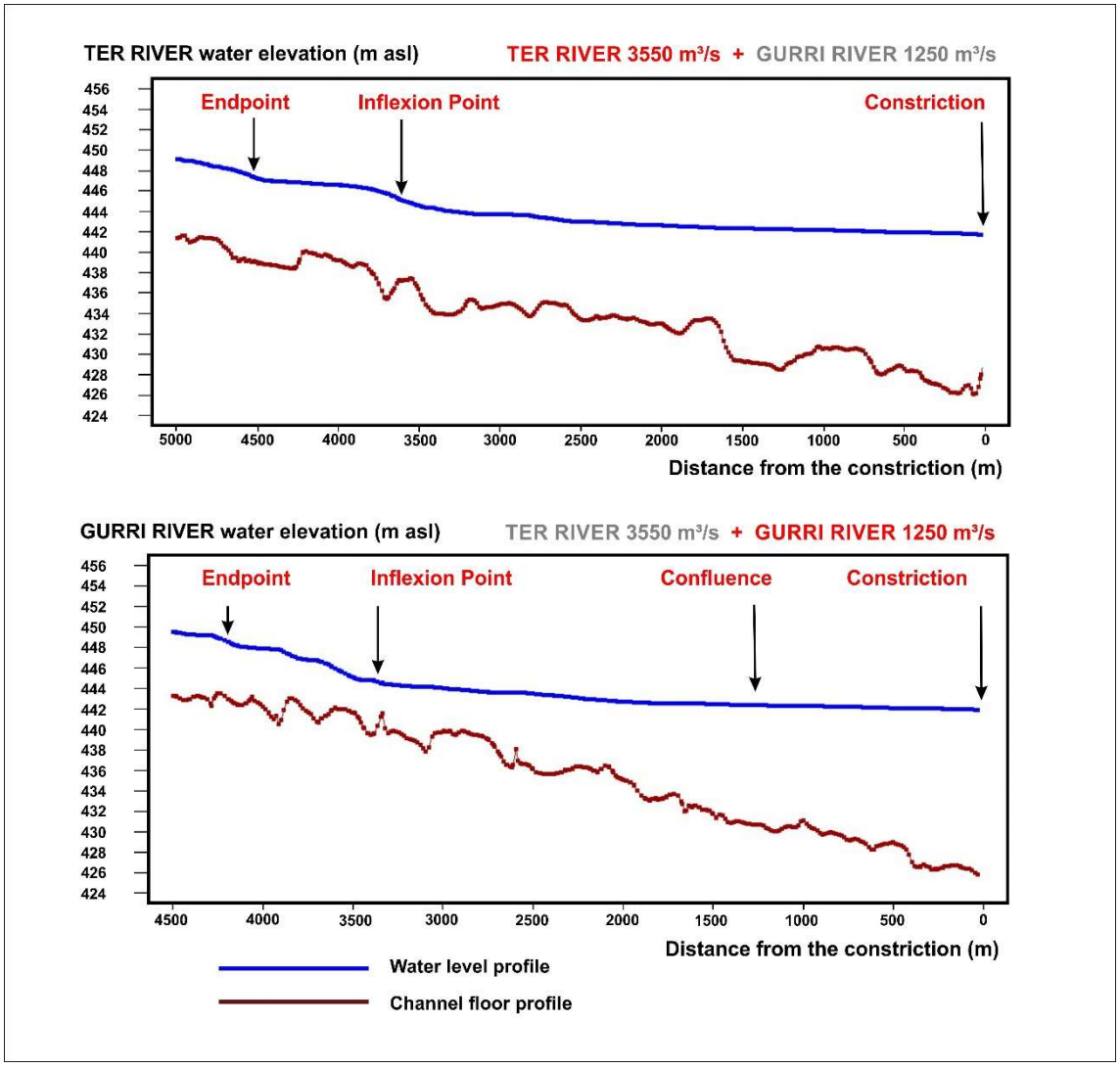

Fig. 8. Profile of the channel bottom and water level between the constriction and the endpoint of the Ter River (above) and the Gurri River (below) during a flood of 3550 m^3/s + 1250 m^3/s (4800 m^3/s at the constriction). The backwater effect extends until the inflexion point of the Ter river's meander. A step between the two zones of the backwater can be recognised at this point. The two separated areas of water storage are the first and second half-meanders. The separation of both zones and the tendency to change the flow condition at the inflexion point indicate disequilibrium. The backwater effect also extends clearly until the inflexion point of the Gurri river's meander. Flow tends to change its condition along the second half-meander until the inflexion point, indicating disequilibrium.

A sequence of flow models was run with the varying water discharge of the main river and the tributary (Table 2). Modelling regards three aspects: water elevation at both endpoints, the reach of the backwater effect, and variations of the flow condition in inflexion points. The modelling in this study sought to find a combination of water discharges from the two rivers to obtain a balanced discharge pattern considering three prior premises. A balanced mixture of water discharges first emerged, increasing of 52% the Q_{500} value at the constriction (Fig. 9). The main river contributed with 5800 m^3/s, while the tributary with 1200 m^3/s.

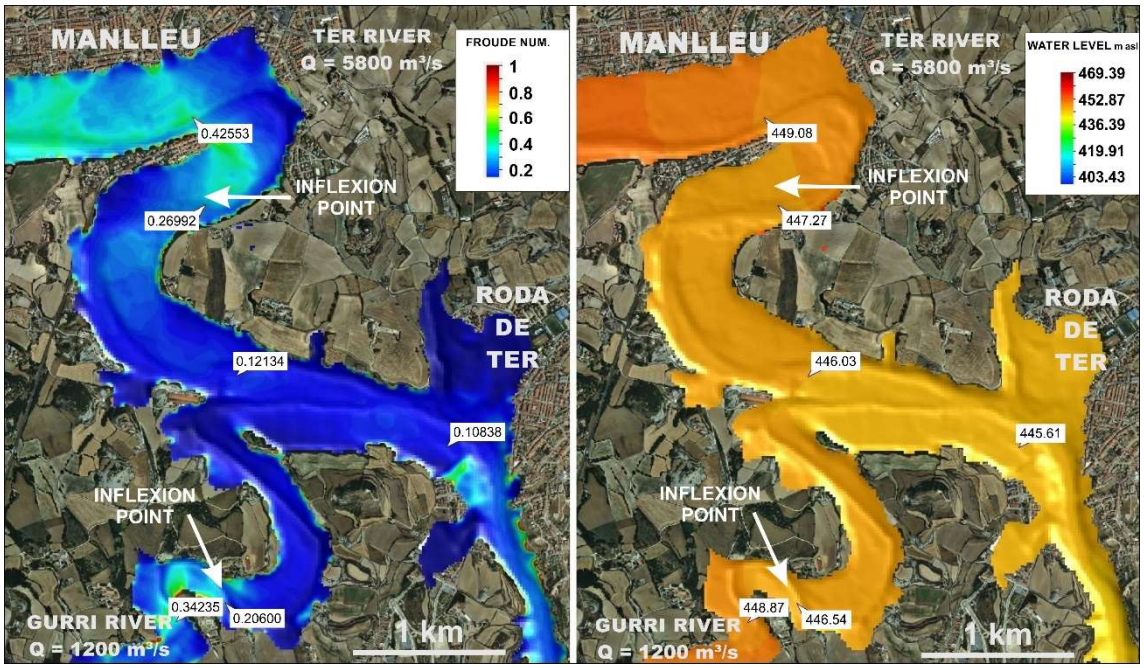

Fig. 9. The Ter River is at a high stage at the constriction. The water discharge mixture is 52% higher (7000 m^3/s) than Q_{500}. The discharge pattern seems to be at equilibrium. Water elevations in the areas of the endpoints are balanced. Moreover, local phenomena developed poorly at the inflexion points, and the step that separates the two half-meanders blurs. This discharge pattern marks the beginning of the pool level.

Equilibrium of water levels at the endpoints was nearly completed, and local phenomena and values of the Froude number achieved low values in the area of the backwater effect from the constriction to the endpoints. The backwater effect reaches the inflexion point of both meanders. This discharge pattern marks the beginning of the pool level, because the step that separates the two half-meanders is blurred (Fig. 10).

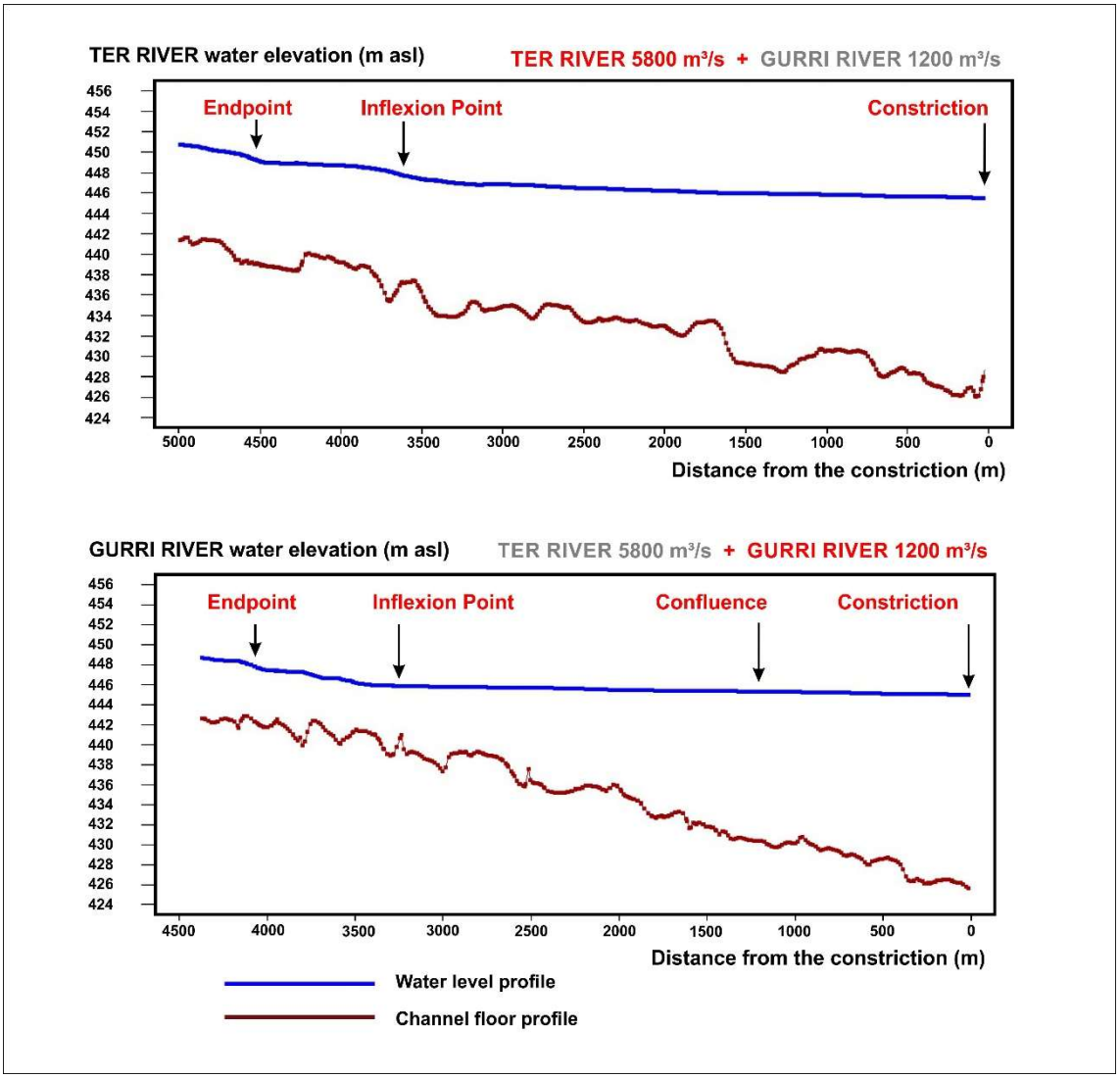

Fig. 10. Profile of the channel bottom and water level between the constriction and endpoint of the Ter River (above) and the Gurri River (below) during a flood of 5800 m^3/s + 1200 m^3/s (7000 m^3/s at the constriction). The backwater effect extends clearly until the inflexion point of the Ter river's meander. The step between the two zones of backwater is blurred in this area. The water elevation of both zones, from the constriction until the inflexion point and from the inflexion point until the endpoint, are reported in Table 2. The backwater effect also extends upstream beyond the inflexion point of Gurri river's meander. The water elevation tends to incline towards horizontality along the second half-meander between the inflexion point and the endpoint. The slope values of the two channel segments are presented in Table 2.

The key to this pattern is the peak of discharge that arrives at the constriction and the combination of discharges of the two streams to produce this peak at the constriction. As presented in Table 2, variations in the mixture of both discharges also result in differences in the values of water elevation and the Froude number at significant points.

Q_{TOTAL} m^3/s	Q_{Ter} m^3/s	Q_{Gurri} m^3/s	Ratio Q	Water Level Endpoint Ter river (m asl)	Water Level Endpoint Gurri river (m asl)	Water Levels Diff. (m)	Water Level Constriction (m asl)	Gradient Endp. - Constr. Ter river	Gradient Endp. - Constr. Gurri river	Gradient Diff. (m)
Manning 0.08										
6900	5650	1250	4.52	449.63	449.44	0.19	446.30	0.000747	0.00073	0.000016
4800	3550	1250	2.84	447.50	449.15	-1.65	442.58	0.001103	0.001528	-0.000425
Manning 0.07										
9100	7650	1450	5.27	451.01	450.26	0.75	448.61	0.000538	0.000384	0.000154
8700	7350	1350	5.44	450.68	450.07	0.61	448.01	0.000599	0.000479	0.000120
8600	7250	1350	5.37	450.60	449.93	0.67	447.91	0.000603	0.000470	0.000133
8350	7000	1350	5.18	450.35	449.77	0.58	447.59	0.000619	0.000507	0.000112
8250	6800	1450	4.68	450.14	449.93	0.21	447.45	0.000603	0.000577	0.000026
8050	6800	1250	5.44	450.05	449.41	0.64	447.14	0.000652	0.000528	0.000125
7250	6000	1250	4.80	449.35	449.12	0.23	445.98	0.000756	0.000730	0.000025
7000	5800	1200	4.83	449.08	448.87	0.21	445.61	0.000778	0.000758	0.000020
6900	5650	1250	4.52	449.05	449.12	-0.07	445.46	0.000805	0.000851	-0.000046
6800	5700	1100	5.18	448.95	448.71	0.24	445.32	0.000814	0.000788	0.000026
5900	5000	900	5.55	448.33	448.36	-0.03	443.80	0.001016	0.001060	-0.000045
4800	3550	1250	2.84	447.24	449.02	-1.78	441.84	0.001211	0.001670	-0.000459
Manning 0.06										
8050	6800	1250	5.44	449.37	448.91	0.46	446.14	0.000724	0.000644	0.000080
7150	5900	1250	4.72	448.48	448.86	-0.38	444.84	0.000816	0.000935	-0.000119
6900	5650	1250	4.52	448.36	448.85	-0.49	444.47	0.000872	0.001019	-0.000146
5750	4500	1250	3.60	447.42	448.82	1.40	442.61	0.001078	0.001444	-0.000366
4800	3550	1250	2.84	446.69	448.60	-1.91	440.94	0.001289	0.001781	-0.000492
Manning 0.045										
8050	6800	1250	5.44	448.23	448.56	-0.33	444.30	0.000881	0.000991	-0.000110
6900	5650	1250	4.52	447.54	448.25	-0.71	442.60	0.001108	0.001314	-0.000206
4800	3550	1250	2.84	446.16	448.61	-2.45	439.42	0.001511	0.002137	-0.000626
Variable Manning 0.04-0.08										
6900	5650	1250	4.52	446.63	448.82	-2.19	438.26	0.001877	0.002456	-0.000579

Table 2. Sensitivity analysis of the variations in the patterns of the discharge patterns around the hydraulic equilibrium. Changes in the mixture of both discharges result in differences in the values of water elevation and Froude number at key points. The comparison between the results obtained by applying different coefficients of Manning in the flow model is significant. The results from three distinct roughness coefficients can be compared. Alternatively, the results from modelling with two areas with different coefficients are presented at the end of the table.

4.4 Water level profile analysis

The water level profile analysis supported the location of the endpoint and, at the same time, evaluated the water storage distribution caused by the backwater effect. In some cases, numerical modelling was conducted with water discharge values below the virtual pool level. Water storage was not homogeneous from the constriction to the endpoint of the backwater effect. The water level profile analysis shows the river reaches with the greatest efficiency of water storage.

As depicted in Figure 11, a case out of the equilibrium state, the backwater effect in the Ter River is divided into two steps. When the water level profile does not reach the pool level, both steps are separated by a hydraulic jump, implying that the modelled examples

showing local phenomena are not in the equilibrium state. Water storage areas are stepped between the two half-meanders. The first step stretches from the constriction to the inflexion point (first half-meander), and the second step fills the second half-meander. The bend of every half-meander contributes to the lowering of water velocity and backing up of water and consequently to water storage. The main backwater effect occurs just upstream from the constriction, but here the effect is only partial. All the partial effects, from this point till the endpoint, have to be added to achieve the whole effect. The effect becomes less apparent with every successive step and blurs as it approaches the endpoint. In this case, local phenomena can appear in the area of the inflexion point of the meander in the form of hydraulic drops and jumps, separating the channel reaches of subcritical flow where the backwater effect and water storage has developed.

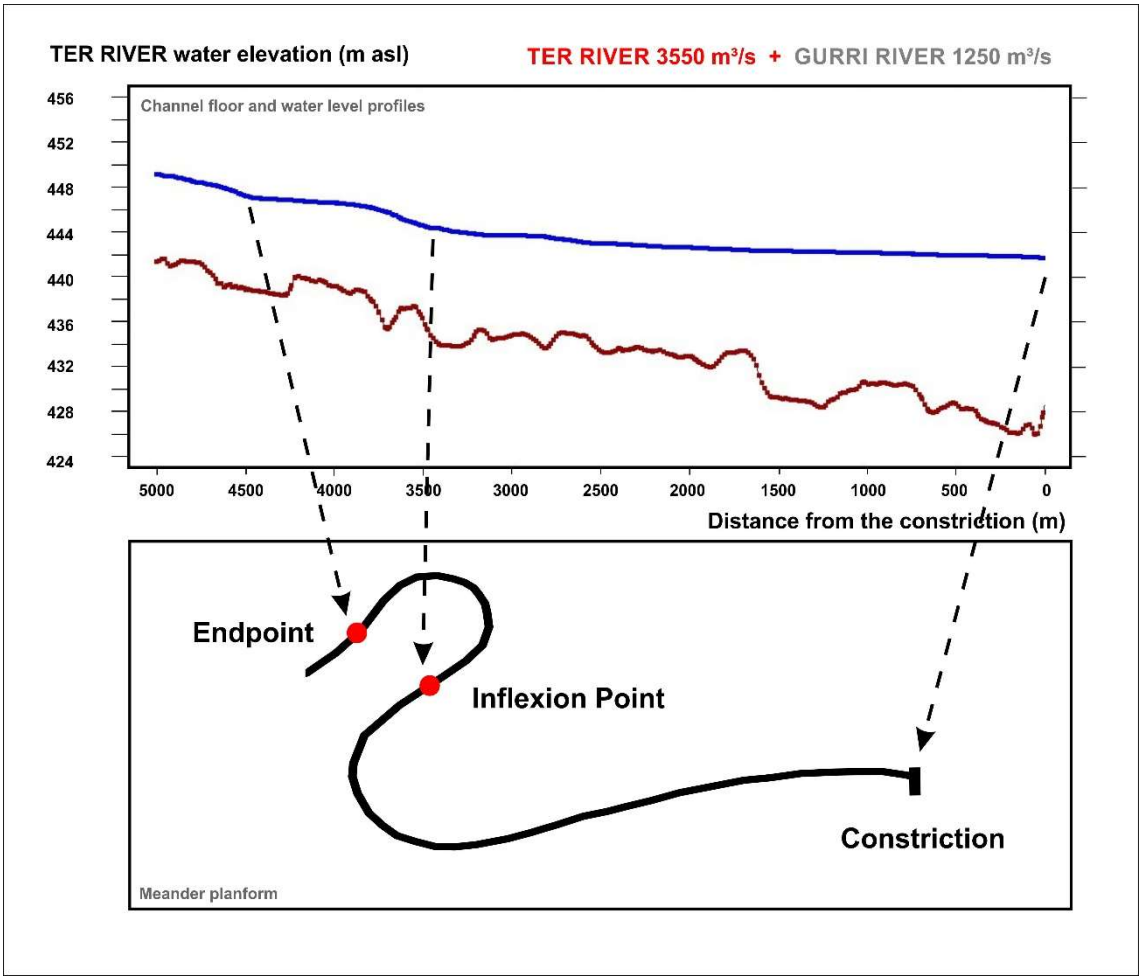

Fig. 11. Water level profile of the Ter River upstream from the constriction. In cases below the pool level, the backwater effect is divided into two steps. Both steps can be separated by a hydraulic jump at the inflexion point. This detail implies that modelled examples showing local phenomena are not in the equilibrium state. The first step extends from the constriction to the inflexion point of the meander (the first half-meander), while the second step fills the second half-meander.

4.5 Discussion

The analysis of the two meanders does not simulate their real evolution in the study area. Meander progression cannot be performed without thorough model calibration, as there are too many unknowns about the former geometry and the sediment transport process

besides some significant simplifications or assumptions, like the use of an adequate bedload transport formula. In this case, Iber used the Meyer-Peter and Müller (1948) formula. Nevertheless, it can be inferred from the results that a two-dimensional numerical model, based on shallow water equations and extended with the effect of secondary currents, can qualitatively explain a morphological evolution, leading to the formation of meanders upstream from the constriction but no further than the endpoint.

The last inference is crucial, since it permits the separation of the origin of the first meander upstream from the constriction of the remaining meanders upstream from it (Fig. 1). In the La Plana de Vic area, the meandering channel pattern of the Ter River goes further upstream from the first meander. Although it was created as the effect of a backwater iteration at the constriction, the previous meanders are not directly related to the constriction effect, but they are related to the constriction position. The meander belt that developed in the Ter River oriented north to south is related to the bend that turns the river's course towards the east. This bend is unavoidable, as it leads the strike drainage system to the drainage basin outlet. As depicted in Figure 3, a channel bend can trigger meander formation.

The presence of the tributary near the constriction is essential. Until the area near the confluence, its channel pattern is predominantly straight, but it changes just before the junction, developing a meander that takes a form comparable to that displayed by the main river. The presence of the two landforms just upstream from the constriction seems to point to its role in developing the formation process. The meandering channel pattern begins at the constriction, because it changes the flow regime and transmits its consequences upstream due to the backwater effect. It is noteworthy to observe that at this point, geomorphology influences hydraulics to a high degree and, at the same time, hydraulics transform geomorphology.

Moreover, the process of meander initiation does not occur downstream from this point but upstream from it. The backwater effect transforms the channel pattern that retains and backs up the flood wave energy. Although water typically flows downslope, water energy can make it flow upstream, as proved by the meander of the tributary. This must have been created by a process running upstream. There is no other comparable meander in channel pattern and width in the course of the tributary. Lastly, the orientation of the tributary's meander shows that its development required the contribution of the main river water discharge, because helical flow works at a high stage, and when it is achieved, the tributary's mouth aligns with a junction point farthest from the constriction.

Another critical question that arises is regarding the triggering of the process. As seen in Figures 1 and 2, the process of meander formation at the constriction works in the described way, at least since formation of terrace T8. From this relative age to the present-day, the confluence has shifted from point C8 to C1, forcing the strike valley outlet into a narrow gorge. From T8 to T4, the terrace remnant distribution is unrelated to the current incised floodplain. T3 is the first terrace connectable with the recent floodplain. T3 and the floodplain are aligned, but the floodplain incises into T3 currently, therefore, the present-day meander configuration must be posterior to T3. The presence of T2 and T1 into the current incised floodplain reinforces the previous interpretation. Hence, the new

meander configuration dates at least from T2. Without absolute terrace dating is difficult to assign a reliable incision rate to the process.

The arriving flood waves to the constriction have been recurrent, since that time has reiterated the process of triggering helical flows upstream from it until the creation of equilibrated meander configuration. Focusing on meander equilibrium, the hydraulic tests performed in the present study analyses in detail the water discharge mixtures from both rivers and other significant variables that have influenced the reaching of the hydraulic equilibrium.

The most significant variable that can break or transform the hydraulic equilibrium at the present-day sinuous planform of the Ter River and its tributary is the roughness coefficient. Since extreme events involve a significant component of overbank flow and floodplains may vary their roughness due to the quantity and quality of the vegetation growing there, this factor is significant in a long-term basis analysis such as the one proposed here. González-Sampériz et al. (2013) inform of terrestrial vegetation changes in the north-eastern Iberian Peninsula during the last 130,000 years. Therefore, the analysis included several Manning's coefficients of roughness.

As climate changes have been able to change the afforestation conditions of floodplains, modelling was run with Manning's coefficients, ranging from that corresponding to a bare channel (0.045) to those applicable to forested and semi-forested conditions (0.08, 0.07, 0.06). Moreover, a double Manning's coefficient, 0.04 for channel areas and 0.08 for floodplains, has been applied. Most of the modelling was run with the value of 0.07, which was the area weighted value between 0.08 and 0.045.

The results exhibited in Table 2 show different aspects. Hydraulic equilibrium is not a precise value of water discharge. The hydraulic balance at the endpoints start, in the case of a roughness coefficient of 0.07, around a water discharge of 5900 m^3/s, and it advances until 8250 m^3/s. Between these two values, the equilibrium moves approximately of 0.2 m. The transit of water discharges from the lower to higher values implies a ratio of discharges between the main river and the tributary over 5, for the lower, and under 5 for the higher values. At this range of water discharges, the water level is considered to be at the pool level. In this situation, water elevation slopes and the slope difference between the main river and the tributary must be the lowest.

The water level gradient between the endpoint of the Ter River and the constriction ranges from 1‰ for the lowest water discharge and 0.6‰ for the highest. The gradient range between the same values in the case of the Gurri River.

At equilibrium, roughness is inversely proportional to the water discharge at the constriction. Equilibrium is maintained not just by decreasing the discharge but also by increasing the roughness. This can be seen through the example of the water discharge of 6900 m^3/s, which is present in all the blocks of the roughness coefficient in Table 2. The decrement of roughness agrees with the decrement of the water elevation at the endpoints, as there is an increase in flow velocity. Since roughness depends on the vegetation present on the floodplain, it confirms that riparian afforestation or deforestation can exert an

impact on the hydraulic equilibrium as well as basin hydrology. Riparian vegetation is one of the factors Lazarus and Constantine (2013) refer to for generating sinuosity.

The inclusion of a double coefficient of roughness in the model, differentiating the channel area and the floodplain area, yields results in the equilibrium state. Flow velocity is higher in the main river, and it produces a falling of the water level at the endpoint. In order to reach equilibrium, the water discharge of the main river must be higher than the 5650 m^3/s modelled and the discharge at the constriction higher than 6900 m^3/s. These discharges were not necessarily caused by meteorological floods, as the headwaters of the Ter River are on glacier areas (Calvet et al., 2011) and, therefore, floods might had been supplied also from glacial lake outburst.

The convergence analyses offer another significant aspect of roughness: models have run with roughness coefficients of 0.06, and the result separated the hydraulic endpoint upstream from the geomorphic one in both cases. Modelling can approach the hydraulic endpoint to the geomorphic endpoint by reducing the coefficient values. It can increment flow velocity, and, as a result, water level at the hydraulic endpoint would go downstream approximating to the geomorphic endpoint. This means ideal circumstances of meander formation under the conditions of bare floodplain or deforestation, which implies lower roughness coefficients and higher flow velocity.

5. Conclusions

Hydraulic parameters controlling the process of the backwater effect in a channel bed and the floodplain of a river system can be reproduced using a 2-dimensional numerical model. This procedure allows to find the reach (endpoint) of the effect upstream from the constriction, values of peak discharges from the two rivers in the hydraulic equilibrium, and the fitting of the hydraulic parameters in the channel reach planform and profile.

The effect of backwater upstream from a lithological constriction can result in sinuosity. The arrangement of channel reaches before and after the constriction generates secondary flows that are transmitted backwards by the backwater effect. This process developed the same sinuous pattern in the Ter River and its tributary, the Gurri River, in La Plana de Vic area (NE Iberian Peninsula) since the Upper Pleistocene.

Hydrodynamic equilibrium requires the contribution of both the rivers. In cases where the backwater effect occurrence affects two rivers, it is essential to evaluate the contribution of each river, because they affect each other. Hydraulic equilibrium can also be modified by riparian vegetation, as it contributes to a reduction of flow velocity. Sudden variations in flow velocity, such as those produced by floodplain afforestation or deforestation, can separate the positions of the hydraulic and geomorphic endpoints.

Calculated discharges can be very helpful when compared with measured meteorological discharges from historical and systematic records. The peak discharges calculated in the case study were never measured in the area, and they are approximately 50% higher than the Q_{500} values, implying that the related flood needs different conditions than the ones characterizing the last centuries. This analysis is relevant because it is thought on a long-term basis, and since the Upper Pleistocene the hydrologic regime of the basin has changed.

The method shows areas where the water storage is effective and how they expand with an increase in water discharge. The numerical flow modelling procedure can be applied to other scenarios that also create the backwater effect and sinuosity, such as river junctions, abrupt changes in slopes, sediment aggradation, or fixed base levels (lakes, dams, seas) to explain geomorphological channel changes.

6. References

Azinfar, H., Kells, J.A., 2011. Drag force and associated backwater effect due to an open channel spur dike field. Journal of Hydraulic Research 49, 248–256.

Baghlani, A., 2012. Application of a high-resolution scheme in simulation of flow in curved channel using boundary–fitted curvilinear coordinates. Scientia Iranica, Elsevier B.V. 19(6),1463–1472.

Becat, J., Soutadé, G., 1990. L'aiguat del 40. Inundacions catastròfiques i polítiques de prevenció a la Mediterrània nord-occidental. Generalitat de Catalunya, Departament de Política Territorial i Obres Públiques. Servei Geològic de Catalunya, Barcelona, 484 pp.

Bladé, E., Cea, L., Corestein, G., Escolano, E., Puertas, J., Vázquez-Cendón, E., Dolz, J., Coll, A., 2014a. Iber: herramienta de simulación numérica del flujo en ríos. Revista Internacional de Métodos Numéricos para Cálculo y Diseño en Ingeniería 30, 1–10.

Bladé, E., Cea, L., Corestein, G., 2014b. Modelización numérica de inundaciones fluviales. Numerical modelling of river inundations 18, 71–82.

Blanckaert, K., de Vriend, H. J., 2010. Meander dynamics: A nonlinear model without curvature restrictions for flow in open–channel bends. Journal of Geophysical Research 115, P04011.

Blondeaux, P., Seminara., G., 1985. A unified bar–bend theory of river meanders. Journal of Fluid Mechanics 157, 449–470.

Brandimarte, L., Woldeyes, M.K., 2013. Uncertainty in the estimation of backwater effects at bridge crossings. Hydrological Processes 27, 1292–1300.

Braudrick, C. A., Dietrich, W. E., Leverich, G. T., Sklar, L. S., 2009. Experimental evidence for the conditions necessary to sustain meandering in coarse–bedded rivers. Proceedings of the National Academy of Sciences of U. S. A. 106 (40), 16936–16941.

Calvet, M., Delmas, M., Gunnell, Y., Braucher, R., Bourlès, D., 2011. Chapter 11–Recent Advances in Rresearch on Quaternary Glaciations in the Pyrenees. In: Ehlers, J., Gibbard, P. L., Hughes, P. D. (Eds.), Developments in Quaternary Sciences, Elsevier, Volume 15, 127–139.

Camporeale, C., Perona, P., Porporato, A., Ridolfi, L., 2007. Hierarchy of Models for Meandering Rivers and Related Morphodynamic Processes. Review of Geophysics 45, 1–28.

Castelltort, F. X., 2017a. Mapa Geològic de Catalunya 1:25.000. Full 73-24 (Manlleu) Geologia del Quaternari. Institut Cartogràfic i Goelògic de Catalunya (ICGC).

Castelltort, F. X., Balasch, J. C., Cirés, J., Colombo, F., 2017b. Consecuencias de la migración lateral de una cuenca de drenaje (Homoclinal shifting) en la formación de la cuenca erosiva de la Plana de Vic. NE de la Cuenca del Ebro. Geogaceta 61, 55–58.

Castillo, C., Pérez, R., Gómez, J.A., 2014. A conceptual model of check dam hydraulics for gully control: Efficiency, optimal spacing and relation with step–pools. Hydrology and Earth System Sciences 18, 1705–1721.

Catalan Water Authority (ACA), 2017. Available at: http://aca-web.gencat.cat/sig/wms/PUBLIC/CABALS/MapServer/WMSServer; 28th July 2017

Catalan Cartographical Authority (ICGC), 2017. Available at: http://www.icc.cat/vissir3/ 28th July 2017

Cea, L., Bladé, E., 2015. A simple and efficient unstructured finite volume scheme for solving the shallow water equations in overland flow applications. Water Resources Research 51, 5464–5486.

Cea, L., Bermudez, M., Puertas, J., Blade, E., Corestein, G., Escolano, E., Conde, A., Bockelmann-Evans, B., Ahmadian, R., 2016. IberWQ: new simulation tool for 2D water quality modelling in rivers and shallow estuaries. Journal of Hydroinformatics 18, 816–830.

Chow, V. T., 1959. Open-channel hydraulics. McGraw-Hill Book Company, 728 pp.

Crosato, A., 2009. Physical explanations of variations in river meander migration rates from model comparison. Earth Surface Processes and Landforms, 34. 2078–2086.

Deltares, 2014. Delft3D-FLOW, User Manual, 710 pp.

De Vriend, H. J., 1987. Analysis of horizontally two–dimensional morphological evolutions in shallow water. Journal of Geophysical Research 92(C4), 3877.

Edwards, B. F., Smith, D. H., 2002. River meandering dynamics. Physical Review E 65, 045303.

Etoh, T., Murota, A., Nakanishi, M., 1986. Exponential Type Distribution of Maximum. Proceedings of International Symposium on Flood Frequency and Risk Analysis. Louisiana (SA), May 1986, 253-265.

Frascati, A., Lanzoni, S., 2009. Morphodynamic regime and long–term evolution of meandering rivers. Journal of Geophysical Research 114, F02002.

Frascati, A., Lanzoni, S., 2010. Long–term river meandering as a part of chaotic Dynamics? A contribution from mathematical modelling. Earth Surface Processes and Landforms 35, 791–802.

González-Sanpériz, p., García-Prieto, E., Aranbarri, J., Valero-Garcés, B. L., Moreno, A., Gil-Romera, G., Sevilla-Callejo, M., Santos, L., Morellón, M., Mata, P., Andrade, A., Carrión, J. S., 2013. Reconstrucción paleoambiental del último ciclo glacial-interglacial en la Iberia continental: la secuencia del Cañizar de Villarquemado (Teruel). Cuadernos de Investigación Geográfica 39 (1), 49-76.

Güneralp, I., Rhoads, B. L., 2010. Spatial autoregressive structure of meander evolution revisited. Geomorphology 120, 91–106.

Hidayat, H., Vermeulen, B., Sassi, M. G., Torfs, P. J., Hoitink, A. J., 2011. Discharge estimation in a backwater affected meandering river. Hydrology and Earth System Sciences 15(8), 2717–2728.

Hooke, J., 2003. River Meander Behaviour and Instability: A Framework for Analysis. Transactions of the Institute of British Geographers 28 (2), 238–253.

Hooke, J., 2007. Complexity, Self–organisation and variation in behaviour in meandering rivers. Geomorphology 91, 236–258.

Hooke, J., Gautier, E., Zolozzi, G., 2011. River meander dynamics: developments in modelling and empirical analyses. Earth Surface Processes and Landforms 36, 1550–1553.

Howard, A. D., Knutson, T. R., 1984. Sufficient Conditions for River Meandering: A Simulation Approach. Water Resources Research 20 (11), 1659–1667.

Howard, A. D., 2009. How to make a meandering river. Proceedings of the National Academy of Sciences of U. S. A. 106 (41), 17245–17246.

Ikeda, S., Parker, G., Sawai, K., 1981. Bend theory of river meanders. Part 1. Linear development. Journal of Fluid Mechanics 112, 363–377.

Johannesson, H., Parker, G., 1989. Linear Theory of River Meanders. In: Ikeda, S. and Parker, G. (Eds.), River Meandering. American Geophysical Union. Water Resources Monograph 12, pp 181–213.

Lazarus, E. D., Constantine, J. A., 2013. Generic theory for channel sinuosity. Proceedings of the National Academy of Sciences of U. S. A. 110 (21), 3447–8452.

Leopold, L. B., Wolman, M. G., 1960. River Meanders. Bulletin of the Geological Society of America 71, 769–794.

Luo, M., Yu, H., Huang, E., Ding, R., Lu, X., 2018. Two-Dimensional Numerical Simulation Study on Bed-Load Transport in the Fluctuating Backwater Area: A Case-Study Reservoir in China. Water 10(10), 1425.

Meyer–Peter, E., Muller, R., 1948. Formulas for bed-load transport. Proceedings of the International Association for Hydraulic Research. Stockholm, 39 pp.

Montalbán, F., Berga, L., Heras, R., Novoa, M., Témez, J.R., 1994. Recomanacions sobre mètodes d'estimació d'avingudes màximes. Junta d'Aigües, Departament de Política Territorial i Obres Públiques, Generalitat de Catalunya, Barcelona, 200 pp.

Naudascher, E., Medlarz, H. J., 1983. Hydrodynamic loading and backwater effect of partially submerged bridges. Journal of Hydraulic Research 21, 213–232.

Ottevanger, W., Blanckaert, K., Uijttewaal, S. J., de Vriend, H. J., 2013. Meander dynamics: A reduced–order nonlinear model without curvature restrictions for flow and bed morphology. Journal of Geophysical Research. Earth Surface 118, 1118–1131.

Parker, G., 1976. On the cause and characteristic scales of meandering and braiding in rivers. Journal of Fluid Mechanics 76 (3), 457–480.

Parker, G., Sawai, K., Ikeda, S., 1982. Bend theory of river meanders. Part 2. Nonlinear deformation of finite–amplitude bends. Journal of Fluid Mechanics 115, 303–314.

Pino, D., Ruiz-Bellet, J. L., Balasch, J. C., Romero-León, L., Tuset, J., Barriendos, M., Mazon, J., Castelltort, X., 2016. Meteorological and hydrological analysis of major floods in NE Iberian Peninsula. Journal of Hydrology 51 (A), 63–89.

Pittaluga, M. B., Nobile, G., Seminara, G., 2009. A non–linear model for river meandering. Water Resources Research 45, W04432.

Pittaluga, M. B., Seminara, G., 2011. Nonlinearity and unsteadiness in river meandering: a review of progress in theory and modelling. Earth Surface Processes and Landforms 36, 20–38.

Rinaldi, M., Mengoni, B., Luppi, L., Darby, S. E., Mosselman, E., 2008. Numerical simulation of hydrodynamics and bank erosion in a river bend. Water Resources Research 44(9), 1–17.

Roe, P.L., 1986. Discrete models for the numerical analysis of time–dependent multidimensional gas dynamics. Journal of Computational Physics 63, 458–476.

Ruiz-Bellet J. L., Castelltort, F. X., Balasch, J.C., Tuset, J., 2017. Uncertainty of the peak flow reconstruction of the 1907 flood in the Ebro River in Xerta (NE Iberian Peninsula). Journal of Hydrology 545, 339–354.

Ruiz–Villanueva, V., Bladé, E., Sánchez–Juny, M., Marti–Cardona, B., Díez–Herrero, A., Bodoque, J.M., 2014. Two–dimensional numerical modeling of wood transport. Journal of Hydroinformatics 16, 1077.

Saif, A., Hosoda, T., 2012. Two–dimensional analysis of flow patterns around a single backward–facing step. International Journal of River Basin Management 10(2), 205–211.

Schumm, S. A., Dumont, J. F., Holbrook, J. M., 2000. Active Tectonics and Alluvial Rivers. Cambridge University Press, Cambridge, 276 pp.

Seminara, G., Zolezzi, G., Tubino, M., Zardi, D., 2001. Downstream and upstream influence in river meandering. Part 2. Planimetric development. Journal of Fluid Mechanics 438, 213–230.

Seminara, G., 2006. Meanders. Journal of Fluid Mechanics 554, 271–297.

Seminara, G., Pittaluga, M. B., 2012. Reductionist versus holistic approaches to the study of river meandering: An ideal dialogue. Geomorphology 163-164, 110–117.

Stolum, H. H., 1996. River Meandering as a Self-organization Process. Science, New Series 271(5256), 1710–1713.

Subramanya, K., 2013. Engineering Hydrology. McGraw Hill, New Dheli, 534 pp.

Stoker, J., 1957. Water Waves, the Mathematical Theory with Applications. Interscience Publishers Inc., New York, 595 pp.

Toro, E. F., 2001. Shock-Capturing Methods for Free–Surface Shallow Flows. John Wiley & Sons, 328 pp.

Vasquez, J.A., Millar, R.G., Steffler, P.M., 2005. River bends and meandering. In: Parker, G. and García, M. (Eds.), River, Coastal and Estuarine Morphodynamics. RCEM, 711–718.

Vázquez–Cendón, M.E., 1999. Improved Treatment of Source Terms in Upwind Schemes for the Shallow Water Equations in Channels with Irregular Geometry. Journal of Computational Physics 148, 497–526.

Vermeulen, B., Hoitink, A. J., Zolezzi, G., Abad, J. D., Aalto, R., 2016. Multiscale structure of meanders. Geophysical Research Letters 43, 3288–3297.

Zolezzi, G., Seminara, G., 2001. Downstream and upstream influence in river meandering. Part 1. General theory and application to overdeepening. Journal of Fluid Mechanics 438, 183–211.